


Magnetoelectric Coupling in Multiferroic Bilayer VS_2

Xingen Liu^{1,2}, Alexander P. Pyatakov,³ and Wei Ren^{1,2,*}

¹Physics Department, Shanghai Key Laboratory of High Temperature Superconductors,
and International Center of Quantum and Molecular Structures, Shanghai University, Shanghai 200444, China

²Materials Genome Institute, and State Key Laboratory of Advanced Special Steel, Shanghai University, Shanghai 200444, China

³Faculty of Physics, M. V. Lomonosov Moscow State University, Moscow 119991, Russia

 (Received 3 November 2019; revised 23 April 2020; accepted 28 October 2020; published 8 December 2020)

Based on the first-principles prediction, we report the magnetoelectric coupling effect in two-dimensional multiferroic bilayer VS_2 . The ground-state $3R$ -type stacking breaks space inversion symmetry, therefore introducing a spontaneous polarization perpendicular to the layer plane. We further reveal that the out-of-plane ferroelectric polarization of bilayer VS_2 can be reversed upon interlayer sliding of an in-plane translation. Each VS_2 layer has a ferromagnetic state with an opposite magnetic moment between two antiferromagnetically ordered layers. We found that ferroelectricity and antiferromagnetism can be coupled together by a ferrovalley in bilayer VS_2 to realize electronic control of magnetism. Remarkably, a net magnetic moment is generated by reducing the interlayer distance, and an electric field is able to achieve linear and second-order nonlinear magnetoelectric coupling in bilayer VS_2 .

DOI: [10.1103/PhysRevLett.125.247601](https://doi.org/10.1103/PhysRevLett.125.247601)

Introduction.—The motion of electrons under the influence of the lattice periodic potential field follows Bloch's theorem. In addition to the two intrinsic properties of charge and spin, Bloch electrons may also have the so-called valley degree of freedom [1–3]. Analogous to ferroelectric (ferromagnetic) materials with spontaneous charge dipole (spin) polarization, systems with spontaneous valley polarization can be referred to as ferrovalley materials [4]. Multiferroic materials with the coexistence of (anti)ferromagnetism, ferroelectricity, ferroelasticity, and ferrovalley, etc., have attracted great attention because of the coupling of different ferroic orderings and the resultant, for instance, magnetoelectric effect [4–7]. In the past decades, multiferroic materials have been studied due to the demand for a new generation of high-performance electronic devices [8–13]. With the rapid rise of two-dimensional materials represented by graphene, more and more new layered structures emerge one after another [14–16]. However, two-dimensional ferromagnetic, ferroelectric, and multiferroic materials of atomic layer thickness are rare, which greatly limits the application of two-dimensional materials with some special multifunctionality. More recently, it has been reported that the electric field might control the valley degree of freedom of the layered material to realize the magnetoelectric effect, where the valley degree of freedom is called pseudospin [17–19]. The existence of two-dimensional ferromagnetic and ferroelectric materials confirmed in experiment will be of great significance for enriching the emergence of two-dimensional materials and developing information technology devices [20–23]. Although several theoretical works predicted that magnetism and ferroelectricity could

coexist in two dimensions, these proposals relied on challenging tasks like doping or absorption, yet both magnetism and ferroelectricity are independent on each other while lacking intrinsic magnetoelectric coupling [24,25]. An interesting two-dimensional compound $\text{Hf}_2\text{VC}_2\text{F}_2$ was studied as a type-II multiferroic in which the intrinsic magnetoelectric coupling was realized [26]. The specific in-plane 120° Y -type antiferromagnetic structure induces ferroelectric polarization which can be fully controlled by magnetic fields, but it is still difficult to achieve electrically controlled magnetism. Furthermore, by twisting the stacking angle between two layers of a bilayer system, the electronic structures and physical properties can be tuned effectively different from the bulk or monolayer counterparts [27,28]. As examples, the monolayer T_d - WTe_2 is not ferroelectric, while bilayer WTe_2 exhibits spontaneous out-of-plane ferroelectric polarization, and its direction could be switched by an external electric field [29]. Bilayer H -phase MoS_2 was also reported to have ferroelectric polarization [30]. And antiferromagnetic bilayer CrI_3 was predicted to show a magnetoelectric response effect [31]. Here, we consider VS_2 with both magnetism and valley on top of polarization, so that the bilayer VS_2 possesses ferroelectricity, ferromagnetism, and ferrovalley at the same time. Through the analysis of electronic structure and Berry curvature (BC), we found that ferroelectricity and antiferromagnetism can be coupled by a ferrovalley to achieve electrically controlled magnetism in bilayer VS_2 , which is of great significance for understanding and manipulating the interaction of electron charge, spin, and valley degrees of freedom.

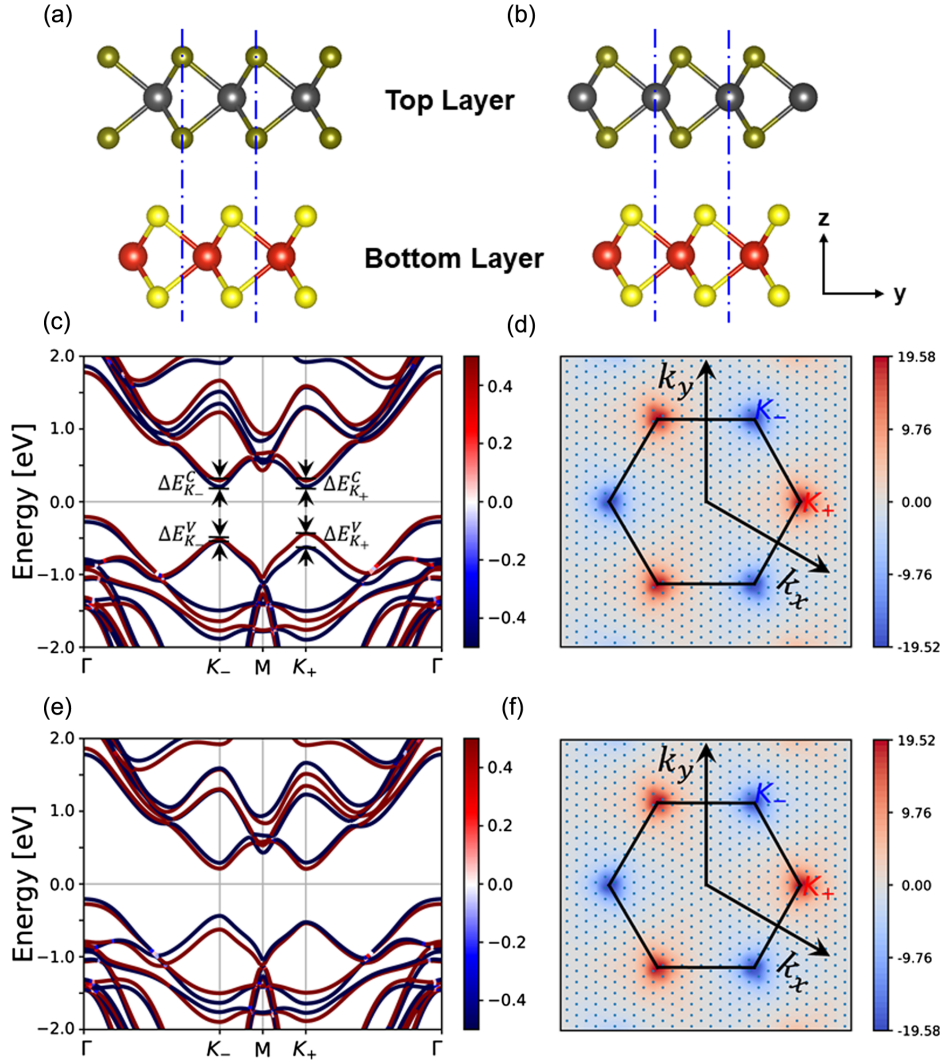


FIG. 1. (a) and (b) are the side views of the bilayer VS₂ crystal structures in which the ferroelectric polarizations are antiparallel and parallel to positive z axes, respectively. The gray and red spheres indicate the top layer and bottom layer V atoms, respectively; the dark yellow and bright yellow spheres are for the top layer and bottom layer S atoms, respectively. The band structure with SOC of ferroelectric antiferromagnetic configurations $P\downarrow M\uparrow\downarrow$ and $P\uparrow M\downarrow\uparrow$ is shown in (c), and the Berry curvature distribution in the first Brillouin zone is shown in (d). The band structure with SOC of configurations $P\downarrow M\downarrow\uparrow$ and $P\uparrow M\uparrow\downarrow$ is shown in (e), and the Berry curvature is shown in (f). In (c) and (e), the red (blue) colors represent the bands of the spin projection in the positive (negative) directions of the z axis (spin up or spin down).

Computational details.—The first-principles density functional theory (DFT) calculations were performed by using the Vienna *ab initio* simulation package (VASP) [32,33]. The projector-augmented wave pseudopotentials method [34] and the generalized gradient approximation (GGA) in the Perdew-Burke-Ernzerhof (PBE) form [35] have been applied. The plane-wave cutoff energy for the wave function was set to be 500 eV. For the geometry optimization, the PBE-D3 method of Grimme with Becke and Johnson damping was considered for taking the van der Waals interaction into account [36,37]. To treat localized d orbitals, we use the GGA + U_{eff} approach introduced by Dudarev *et al.* [38] with $U_{\text{eff}} = 3.0$ eV for V atoms, which has been widely used in previous reports [39–41].

Γ -centered $33 \times 33 \times 1$ Monkhorst-Pack k mesh was adopted for the k -point sampling, and a sufficiently large vacuum distance of 15 Å along the out-of-plane direction was adopted to eliminate interaction between layers. The structures were obtained through structural relaxation until Hellmann-Feynman forces were less than 0.001 eV/Å. The ferroelectric switching pathway was obtained by using the climbing image nudged elastic band method [42], and the ferroelectric polarization value was calculated by using the Berry phase method [43,44]. The external electric field is introduced by using the planar dipole method [45].

Results and discussions.—Consistent with the previous investigation, our calculated results show that the most stable structure of the monolayer VS₂ is the ferromagnetic

H phase with a total magnetic moment of $1\mu_B$ per V atom [40,46,47]. For the bilayer VS_2 case, each layer has a ferromagnetic state with opposite magnetic moments between two antiferromagnetically ordered layers, which is similar to the result of bilayer VSe_2 [48]. However, the most stable bilayer VSe_2 has $2H$ stacking, while in our bilayer VS_2 the ground state is the $3R$ stacking as shown in Fig. 1(a) or 1(b). $2H$ type is a stacked structure with space inversion symmetry, and therefore the ferroelectric polarization is absent; but $3R$ -type stacking breaks space inversion symmetry, therefore showing a spontaneous polarization. Figures 1(a) and 1(b) illustrate the side views of structures in which ferroelectric polarizations are negative and positive in the z axis. Similar to the polarization switching mode in bilayer $\text{T}_d\text{-WTe}_2$ [49,50], the out-of-plane ferroelectric polarization of bilayer VS_2 can be reversed upon interlayer sliding of an in-plane translation. The origin of ferroelectricity is the same as that of $\text{T}_d\text{-WTe}_2$ and $\text{T}_d\text{-MoTe}_2$, due to the different environments of the S atoms at the gap of two layers, forming uncompensated interlayer vertical charge transfer and the out-of-plane dipole (see Supplemental Material [51], Figs. S1 and S2). The ferroelectric polarization value of bilayer VS_2 calculated by using the Berry phase method is $2.018 \times 10^{-3} \text{ C/m}^2$, larger than the experimental reports of $\text{T}_d\text{-WTe}_2$ ($3.204 \times 10^{-4} \text{ C/m}^2$) [29] and $\text{T}_d\text{-MoTe}_2$ ($5.768 \times 10^{-4} \text{ C/m}^2$) [54].

Bilayer VS_2 is thus found to be multiferroic with coexistence of both ferroelectricity and interlayer antiferromagnetism. Therefore, we consider four different configurations, namely, $P\uparrow M\uparrow\downarrow$, $P\uparrow M\downarrow\uparrow$, $P\downarrow M\uparrow\downarrow$, and $P\downarrow M\downarrow\uparrow$ [here, $P\uparrow$ represents the ferroelectric polarization direction toward the positive z -axis direction; $M\uparrow\downarrow$ represents the magnetic moment of bottom (top) layer VS_2 along the positive (negative) direction of the z axis]. Through our DFT calculations, we discover that all four ferroelectric antiferromagnetic configurations are degenerate in energy. The electronic band structures of the ferroelectric bistable states with reversed ferroelectric polarization should also be indistinguishable. The spin projection band structure and BC of all four different configurations with spin orbit coupling (SOC) are shown in Figs. 1(c)–1(f). For two-dimensional honeycomb lattice systems, the extrema of the conduction band and valence band have the same wave vector and are distributed at the corners of the hexagonal Brillouin zone K_+ and K_- [2]. The band structures near the extreme points are called energy valleys K_+ and K_- , which are related to each other by time reversal symmetry and cannot be converted by translational symmetry.

The $P\downarrow M\uparrow\downarrow$ and $P\uparrow M\downarrow\uparrow$ configurations have the same band structure as shown in Fig. 1(c), and the BC distribution in the first Brillouin zone is shown in Fig. 1(d). The same band structures of $P\downarrow M\downarrow\uparrow$ and $P\uparrow M\uparrow\downarrow$ configurations are shown in Fig. 1(e), and their BC distribution is shown in Fig. 1(f). Owing to the interaction of the interlayer

ferrovalley, the splitting values at the bottom of the conduction band and the top of the valence band are not equal at K_+ and K_- points (in contrast to the monolayer or two well-separated bilayers in Supplemental Material [51], Figs. S3 and S4). Quantitatively, $P\downarrow M\uparrow\downarrow$ and $P\uparrow M\downarrow\uparrow$ configurations have energy splittings $\Delta E_{K_+}^V = 0.013 \text{ eV}$, $\Delta E_{K_+}^C = 0.188 \text{ eV}$, $\Delta E_{K_-}^C = 0.086 \text{ eV}$, and $\Delta E_{K_+}^C = 0.078 \text{ eV}$; whereas for $P\downarrow M\downarrow\uparrow$ and $P\uparrow M\uparrow\downarrow$ configurations, $\Delta E_{K_-}^V = 0.188 \text{ eV}$, $\Delta E_{K_+}^V = 0.013 \text{ eV}$, $\Delta E_{K_-}^C = 0.078 \text{ eV}$, and $\Delta E_{K_+}^C = 0.086 \text{ eV}$. So we can clearly see that, for the band structures of $P\downarrow M\uparrow\downarrow$ and $P\uparrow M\downarrow\uparrow$ configurations, the spin projection of the topmost valence band is spin up, and the bottom conduction band is spin down; while in the band structure of $P\downarrow M\downarrow\uparrow$ and $P\uparrow M\uparrow\downarrow$ configurations, the spin projections are completely reversed. For valley materials, the energy valleys K_+ and K_- are related to each other by time reversal symmetry rather than translational symmetry [2]. It might be thought that, when the bilayer VS_2 ferroelectric polarization is switched, the direction of magnetic moments in the top and bottom VS_2 layers needs to flip 180° to keep the band structure unchanged. From the perspective of qualitative definition of band structure, the spin projection, and the influence of an external electric field (see Supplemental Material [51], Figs. S5 and S6), this is our first evidence that ferroelectric control of magnetism is achieved by ferrovalley coupling in bilayer VS_2 .

Berry curvature can be regarded as a pseudomagnetic field in momentum space. In general, the magnetic field is written as the cross-product of the vector differential operator and the magnetic vector potential $B(\vec{r}) = \nabla \times A(\vec{r})$, and the definition of BC is in similar form: $\Omega_n(\vec{k}) = \nabla \times C_n(\vec{k})$ [55–57]. Here, n is the band index, $C_n(\vec{k}) = i\langle u_n(\vec{k}) | \nabla_{\vec{k}} | u_n(\vec{k}) \rangle$ represents Berry connection, and $u_n(\vec{k})$ is the periodic part of the Bloch wave function. We know that the electrostatic field is an irrotational field, and its curl is zero: $\nabla \times \vec{E} = 0$. Before proceeding to further analysis and discussion, it is necessary to emphasize that we have considered the sum of the BC values (“global” BCs) for all the electron occupied bands below the Fermi level. Consistent with the H -phase VSe_2 ferrovalley [4], monolayer H -phase VS_2 also has spontaneous valley polarization, such that the absolute BCs between the two energy valleys are no longer equal. As shown in Fig. 1(d), the BCs of $P\downarrow M\uparrow\downarrow$ configuration at K_- is -19.52 \AA^{-2} and 19.58 \AA^{-2} at K_+ . Because of the interlayer interaction, their absolute values are slightly larger than those when the interlayer interaction is absent (see Supplemental Material [51], Figs. S3 and S4). When the magnetic moments are reversed to $P\downarrow M\downarrow\uparrow$ configuration, as shown in Fig. 1(f), the BC at K_- is -19.58 \AA^{-2} and 19.52 \AA^{-2} at K_+ . While the ferroelectric polarization is switched with the magnetic moment unchanged, namely, $P\uparrow M\uparrow\downarrow$ configuration, the BC at K_- is -19.58 \AA^{-2} and 19.52 \AA^{-2} at K_+ which is consistent with the results of $P\downarrow M\downarrow\uparrow$ configuration.

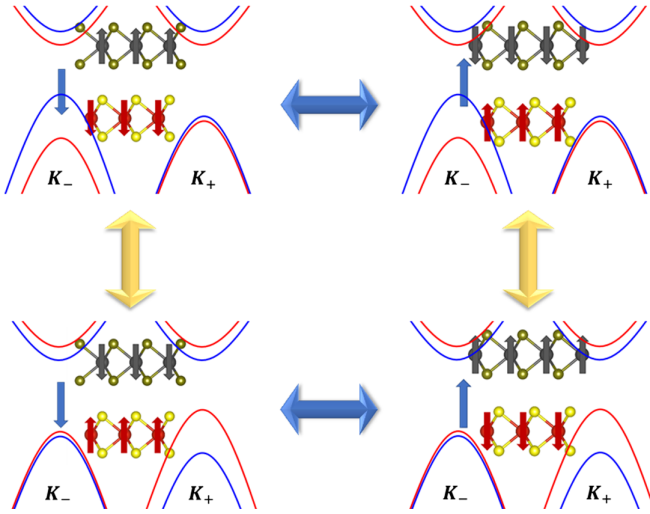


FIG. 2. Multistate control of two-dimensional multiferroic bilayer VS_2 . The red and gray arrows represent the spin directions of the bottom layer and top layer VS_2 , respectively. The blue arrows represent the ferroelectric polarization direction of the system. At the two energy valleys K_- and K_+ , red and blue curves represent bands where the spin projection is positive (spin-up) and negative (spin-down) along the z axis, respectively.

According to Table S1 [51], regardless of monolayer or bilayer VS_2 , the global BCs at K_+ and K_- points do not change with the external electric field and ferroelectric switching. If we consider only the “local” BCs of the highest valence band at the K_-/K_+ point, the external electric field dependences of the BC change for two ferroelectric inversion partners should be opposite [58]. The BC change trends of $P\downarrow M\uparrow\downarrow$ and $P\uparrow M\downarrow\uparrow$ are symmetric, while the BC change trends of $P\downarrow M\uparrow\downarrow$ and $P\uparrow M\uparrow\downarrow$ are irrelevant (see Supplemental Material [51], Fig. S7). Therefore, this means that $P\downarrow M\uparrow\downarrow$ and $P\uparrow M\downarrow\uparrow$ are ferroelectric inversion (bistable) partners, while $P\downarrow M\uparrow\downarrow$ and $P\uparrow M\uparrow\downarrow$ are ferroelectric noninversion partners. From the perspective of the quantitative value of the Berry curvature, we observe that, when ferroelectric polarization P flips between $P\uparrow$ and $P\downarrow$, the magnetic moments in the top and bottom layers of VS_2 should also be reversed between $M\downarrow\uparrow$ and $M\uparrow\downarrow$. This is another evidence that ferroelectric control of magnetism is achieved by ferrovalley coupling in bilayer VS_2 . From our further research, this is not a special case but common in bilayer ferroelectric-antiferromagnetic ferrovalley materials, such as transition metal dichalcogenides VTe_2 and NbSe_2 (see Supplemental Material [51], Figs. S8 and S9 and Table S2).

As shown in Fig. 2, since ferroelectric control of interlayer antiferromagnetism is achieved by ferrovalley coupling in bilayer VS_2 , and the monolayer VS_2 is still ferromagnetic, this suggests that it has significant potential application in a new generation of high-performance electronic functional device. Moreover, we can also switch

the antiferromagnetic structure of bilayer VS_2 by applying an external magnetic field [22] or a magnetic proximity coupling, as shown by the yellow arrows in Fig. 2. In this way, using the external magnetic field and electric field, we can realize arbitrary switching in all four different ferroelectric antiferromagnetic configurations, which provides a new possibility for realizing multistate storage.

Controlling magnetism by using electrical means is one of the key challenges of the next generation of information technology. Recently, it has been reported that a large linear magnetoelectric coupling effect was observed in two-dimensional van der Waals material bilayer CrI_3 [59]. Here, we studied the influence of an external electric field on the magnetism of bilayer VS_2 with different interlayer distance. The detailed effects of the ferroelectric polarization, V–S bond lengths, energy, and force by tuning the interlayer distance are provided in Fig. S10 [51]. As shown in Figs. 3(a) and 3(b), the layer separation (d) has an important effect on the magnetic properties of bilayer VS_2 . As we suppress d from the equilibrium d_0 by a deviation $\delta_d = d_0 - d$, the bilayer VS_2 changes from antiferromagnetism to ferrimagnetism, and the total magnetic moment of the system increases with the increase of δ_d . Furthermore, when $\delta_d = 0.6 \text{ \AA}$, the net magnetic moment changes approximately linearly with a small electric field as shown in Fig. 3(c). The induced magnetization change ΔM depends on the electric field E as $\mu_0 \Delta M = \alpha_S E$, where α_S denotes the linear magnetoelectric coefficient [60]. Here a positive electric field is defined to be along the positive direction of the z axis. From the linear fit to the calculated data, we find that for $P\downarrow M\uparrow\downarrow$ configuration $\alpha_S \approx -9.8 \times 10^{-14} \text{ G cm}^2/\text{V}$ (or $-1.48 \times 10^{-7} \text{ s/m}$ using SI units) and for $P\uparrow M\uparrow\downarrow$ configuration $\alpha_S \approx 9.8 \times 10^{-14} \text{ G cm}^2/\text{V}$ ($1.48 \times 10^{-7} \text{ s/m}$). This magnitude is larger than the Fe slab films $\alpha_S^{001} \approx 2.9 \times 10^{-14} \text{ G cm}^2/\text{V}$ reported in Ref. [60] and 10^5 times larger than Cr_2O_3 $\alpha_\perp = 1.45 \text{ ps/m}$ reported in Ref. [61] or $\alpha_\perp = 1.04 \text{ ps/m}$ reported in Ref. [62]. When $\delta_d = 0.8 \text{ \AA}$, the magnetic moment displays second-order nonlinearity with the electric field as shown in Fig. 3(d). It can be numerically fitted by the formula $\mu_0 \Delta M = \beta_S E^2 + \alpha_S E$, where β_S denotes the second-order nonlinear magnetoelectric coefficient. The numerical values show that for $P\downarrow M\uparrow\downarrow$ configuration $\beta_S \approx -4.5 \times 10^{-22} \text{ G cm}^3/\text{V}^2$ ($= -6.98 \times 10^{-14} \text{ s/V}$) and $\alpha_S \approx -4.8 \times 10^{-14} \text{ G cm}^2/\text{V}$ ($= -7.372 \times 10^{-8} \text{ s/m}$) and for $P\uparrow M\uparrow\downarrow$ configuration $\beta_S \approx -4.5 \times 10^{-22} \text{ G cm}^3/\text{V}^2$ and $\alpha_S \approx 4.8 \times 10^{-14} \text{ G cm}^2/\text{V}$. The rules of $P\downarrow M\uparrow\downarrow$ ($P\uparrow M\downarrow\uparrow$) and $P\downarrow M\downarrow\uparrow$ ($P\uparrow M\uparrow\downarrow$) are the same, for equal absolute values of the total magnetic moments, but opposite signs. In Fig. S11 [51], we present the antiferromagnetic to ferromagnetic transformation of bilayer VS_2 under the external electric field. When the field intensity is greater than 0.7 V/\AA , the ground state of the bilayer changes from antiferromagnetic to ferromagnetic. At the same time, the system is electronically transformed from a semiconductor

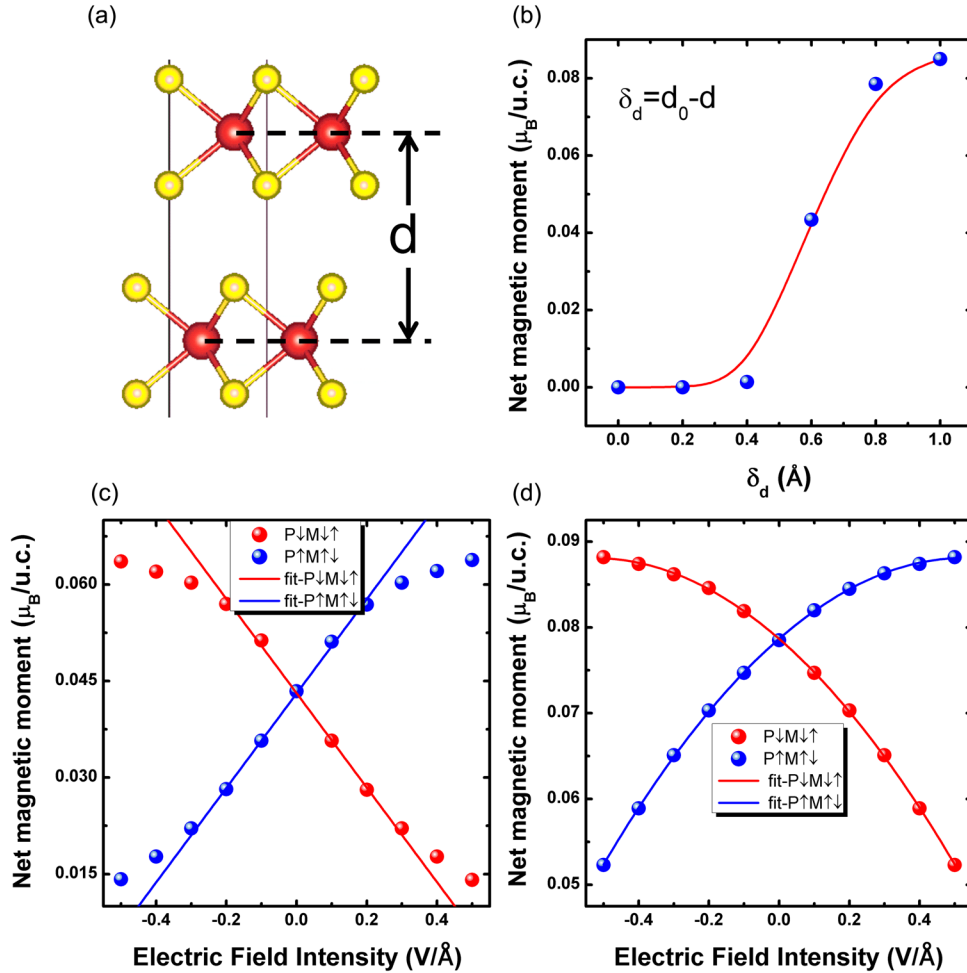


FIG. 3. Total magnetic moments (without SOC) on bilayer VS₂ as a function of the interlayer distance variation and external electric field. The definition of the bilayer VS₂ interlayer distance d is shown in (a), which is the distance between two V atomic layers. The interlayer distance of the equilibrium state obtained through structural optimization is defined as d_0 , and δ_d is the decrease of the interlayer distance d as shown in (b). The net magnetic moment of the bilayer VS₂ system increases with the increase of δ_d . (c) and (d) show the relationship between the net magnetic moments and the external electric field when $\delta_d = 0.6$ and 0.8 \AA , respectively. The red and blue data points and lines are the calculated and fitting results.

to a metal. For completeness, we present the spin projection band structure and BC distribution for the ferroelectric ferromagnetic configurations in Figs. S12 and S13 [51].

In summary, based on the first-principles density functional theory, we studied the magnetoelectric coupling effect in bilayer VS₂ multiferroic material. We found that ferroelectricity and antiferromagnetism in bilayer VS₂ are coupled together by a ferrovalley to achieve electrically controlled magnetism. One can design switching of four different ferroelectric-antiferromagnetic configurations, which provide new possibility for realizing multistate storage. From our further investigation, it is not a special case only for the bilayer 3R VS₂ but is universal in the bilayer ferroelectric-antiferromagnetic ferrovalley materials. Moreover, the interlayer distance has an important effect on the magnetic properties of bilayer VS₂. Furthermore, we can achieve giant linear and second-order

nonlinear magnetoelectric coupling at various interlayer distances. Our investigations reveal a microscopic mechanism of the coexistence and coupling between ferroelectric, antiferromagnetic, and ferrovalley based on the bilayer multiferroic materials, which is of great significance for understanding and manipulating the interaction of electron charge, spin, and valley degrees of freedom.

This work was supported by the National Natural Science Foundation of China (Grants No. 51861145315, No. 51672171, and No. 12074241), Joint Russian Foundation for Basic Research (RFBR) and National Science Foundation of China (NSFC) grant (RFBR No. 19-52-53020 and NSFC No. 51911530124), Shanghai Municipal Science and Technology Commission Program (No. 19010500500), National Key Basic Research Program of China (No. 2015CB921600),

Independent Research Project of State Key Laboratory of Advanced Special Steel, and Shanghai Key Laboratory of Advanced Ferrometallurgy at Shanghai University.

*renwei@shu.edu.cn

- [1] A. Rycerz, J. Tworzydło, and C. W. J. Beenakker, *Nat. Phys.* **3**, 172 (2007).
- [2] D. Xiao, W. Yao, and Q. Niu, *Phys. Rev. Lett.* **99**, 236809 (2007).
- [3] X. Li, T. Cao, Q. Niu, J. R. Shi, and J. Feng, *Proc. Natl. Acad. Sci. U.S.A.* **110**, 3738 (2013).
- [4] W. Y. Tong, S. J. Gong, X. Wan, and C. G. Duan, *Nat. Commun.* **7**, 13612 (2016).
- [5] M. Fiebig, T. Lottermoser, D. Meier, and M. Trassin, *Nat. Rev. Mater.* **1**, 16046 (2016).
- [6] W. Eerenstein, N. D. Mathur, and J. F. Scott, *Nature (London)* **442**, 759 (2006).
- [7] N. A. Spaldin and R. Ramesh, *Nat. Mater.* **18**, 203 (2019).
- [8] C. Israel, N. D. Mathur, and J. F. Scott, *Nat. Mater.* **7**, 93 (2008).
- [9] M. Gajek, M. Bibes, S. Fusil, K. Bouzehouane, J. Fontcuberta, A. Barthelemy, and A. Fert, *Nat. Mater.* **6**, 296 (2007).
- [10] Y. H. Chu, L. W. Martin, M. B. Holcomb, M. Gajek, S. J. Han, Q. He, N. Balke, C. H. Yang, D. Lee, W. Hu, Q. Zhan, P. L. Yang, A. Fraile-Rodriguez, A. Scholl, S. X. Wang, and R. Ramesh, *Nat. Mater.* **7**, 478 (2008).
- [11] F. Zavaliche, T. Zhao, H. Zheng, F. Straub, M. P. Cruz, P. L. Yang, D. Hao, and R. Ramesh, *Nano Lett.* **7**, 1586 (2007).
- [12] J. F. Scott, *J. Mater. Chem.* **22**, 4567 (2012).
- [13] A. P. Pyatakov and A. K. Zvezdin, *Phys. Usp.* **55**, 557 (2012).
- [14] K. S. Novoselov, A. K. Geim, S. V. Morozov, D. Jiang, Y. Zhang, S. V. Dubonos, I. V. Grigorieva, and A. A. Firsov, *Science* **306**, 666 (2004).
- [15] K. F. Mak, C. Lee, J. Hone, J. Shan, and T. F. Heinz, *Phys. Rev. Lett.* **105**, 136805 (2010).
- [16] L. Li, Y. Yu, G. J. Ye, Q. Ge, X. Ou, H. Wu, D. Feng, X. H. Chen, and Y. Zhang, *Nat. Nanotechnol.* **9**, 372 (2014).
- [17] Z. Gong, G. B. Liu, H. Yu, D. Xiao, X. Cui, X. Xu, and W. Yao, *Nat. Commun.* **4**, 2053 (2013).
- [18] S. Wu, J. S. Ross, G.-B. Liu, G. Aivazian, A. Jones, Z. Fei, W. Zhu, D. Xiao, W. Yao, D. Cobden, and X. Xu, *Nat. Phys.* **9**, 149 (2013).
- [19] J. Lee, Z. Wang, H. Xie, K. F. Mak, and J. Shan, *Nat. Mater.* **16**, 887 (2017).
- [20] K. Chang, J. W. Liu, H. C. Li, N. Wang, K. Zhao, A. M. Zhang, F. Jin, Y. Zhong, X. P. Hu, W. H. Duan, Q. M. Zhang, L. Fu, Q. K. Xue, X. Chen, and S. H. Ji, *Science* **353**, 274 (2016).
- [21] Y. Zhou, D. Wu, Y. Zhu, Y. Cho, Q. He, X. Yang, K. Herrera, Z. Chu, Y. Han, M. C. Downer, H. Peng, and K. Lai, *Nano Lett.* **17**, 5508 (2017).
- [22] B. Huang, G. Clark, E. Navarro-Moratalla, D. R. Klein, R. Cheng, K. L. Seyler, D. Zhong, E. Schmidgall, M. A. McGuire, D. H. Cobden, W. Yao, D. Xiao, P. Jarillo-Herrero, and X. Xu, *Nature (London)* **546**, 270 (2017).
- [23] Y. Deng, Y. Yu, Y. Song, J. Zhang, N. Z. Wang, Z. Sun, Y. Yi, Y. Z. Wu, S. Wu, J. Zhu, J. Wang, X. H. Chen, and Y. Zhang, *Nature (London)* **563**, 94 (2018).
- [24] Z. Tu, M. Wu, and X. C. Zeng, *J. Phys. Chem. Lett.* **8**, 1973 (2017).
- [25] Q. Yang, W. Xiong, L. Zhu, G. Gao, and M. Wu, *J. Am. Chem. Soc.* **139**, 11506 (2017).
- [26] J. J. Zhang, L. Lin, Y. Zhang, M. Wu, B. I. Yakobson, and S. Dong, *J. Am. Chem. Soc.* **140**, 9768 (2018).
- [27] Y. Cao, V. Fatemi, A. Demir, S. Fang, S. L. Tomarken, J. Y. Luo, J. D. Sanchez-Yamagishi, K. Watanabe, T. Taniguchi, E. Kaxiras, R. C. Ashoori, and P. Jarillo-Herrero, *Nature (London)* **556**, 80 (2018).
- [28] Y. Cao, V. Fatemi, S. Fang, K. Watanabe, T. Taniguchi, E. Kaxiras, and P. Jarillo-Herrero, *Nature (London)* **556**, 43 (2018).
- [29] Z. Fei, W. Zhao, T. A. Palomaki, B. Sun, M. K. Miller, Z. Zhao, J. Yan, X. Xu, and D. H. Cobden, *Nature (London)* **560**, 336 (2018).
- [30] L. Li and M. H. Wu, *ACS Nano* **11**, 6382 (2017).
- [31] C. Lei, B. L. Chittari, K. Nomura, N. Banerjee, J. Jung, and A. H. MacDonald, *arXiv:1902.06418*.
- [32] G. Kresse and J. Furthmuller, *Comput. Mater. Sci.* **6**, 15 (1996).
- [33] G. Kresse and J. Furthmuller, *Phys. Rev. B* **54**, 11169 (1996).
- [34] P. E. Blöchl, *Phys. Rev. B* **50**, 17953 (1994).
- [35] J. P. Perdew, K. Burke, and M. Ernzerhof, *Phys. Rev. Lett.* **77**, 3865 (1996).
- [36] S. Grimme, J. Antony, S. Ehrlich, and H. Krieg, *J. Chem. Phys.* **132**, 154104 (2010).
- [37] S. Grimme, S. Ehrlich, and L. Goerigk, *J. Comput. Chem.* **32**, 1456 (2011).
- [38] S. L. Dudarev, G. A. Botton, S. Y. Savrasov, C. J. Humphreys, and A. P. Sutton, *Phys. Rev. B* **57**, 1505 (1998).
- [39] L. Wang, T. Maxisch, and G. Ceder, *Phys. Rev. B* **73**, 195107 (2006).
- [40] M. Kan, B. Wang, Y. H. Lee, and Q. Sun, *Nano Res.* **8**, 1348 (2015).
- [41] H. He, H. Gao, W. Wu, S. Cao, J. Hong, D. Yu, G. Deng, Y. Gao, P. Zhang, H. Luo, and W. Ren, *Phys. Rev. B* **94**, 205127 (2016).
- [42] G. Henkelman, B. P. Uberuaga, and H. Jonsson, *J. Chem. Phys.* **113**, 9901 (2000).
- [43] R. D. King-Smith and D. Vanderbilt, *Phys. Rev. B* **47**, 1651 (1993).
- [44] R. Resta, M. Posternak, and A. Baldereschi, *Phys. Rev. Lett.* **70**, 1010 (1993).
- [45] J. Neugebauer and M. Scheffler, *Phys. Rev. B* **46**, 16067 (1992).
- [46] H. Zhang, L. M. Liu, and W. M. Lau, *J. Mater. Chem. A* **1**, 10821 (2013).
- [47] H. L. Zhuang and R. G. Hennig, *Phys. Rev. B* **93**, 054429 (2016).
- [48] W.-Y. Tong and C.-G. Duan, *npj Quantum Mater.* **2**, 47 (2017).
- [49] Q. Yang, M. Wu, and J. Li, *J. Phys. Chem. Lett.* **9**, 7160 (2018).
- [50] X. Liu, Y. Yang, T. Hu, G.-D. Zhao, C. Chen, and W. Ren, *Nanoscale* **11**, 18575 (2019).

- [51] See Supplemental Material at <http://link.aps.org/supplemental/10.1103/PhysRevLett.125.247601>, which includes Refs. [52,53], for (i) ground state properties of bilayer 3R-stacking VS₂; (ii) band structures and BCs of monolayer VS₂ and bilayer VS₂ without interlayer interaction; (iii) band structures and BCs of bilayer VS₂ under an external electric field; (iv) magnetoelectric coupling examples in other 2D FE-AFM-ferrovalley materials; (v) interlayer distance effect on the properties of bilayer VS₂; and (vi) band structures and BCs of bilayer VS₂ FE-FM configurations.
- [52] G. Mills, H. Jonsson, and G. S. Schenter, *Surf. Sci.* **324**, 305 (1995).
- [53] D. Di Sante, A. Stroppa, P. Barone, M. H. Whangbo, and S. Picozzi, *Phys. Rev. B* **91**, 161401(R) (2015).
- [54] F. T. Huang, S. J. Lim, S. Singh, J. Kim, L. Zhang, J. W. Kim, M. W. Chu, K. M. Rabe, D. Vanderbilt, and S. W. Cheong, *Nat. Commun.* **10**, 4211 (2019).
- [55] D. Xiao, M.-C. Chang, and Q. Niu, *Rev. Mod. Phys.* **82**, 1959 (2010).
- [56] H.-J. Kim, C. Li, J. Feng, J.-H. Cho, and Z. Zhang, *Phys. Rev. B* **93**, 041404(R) (2016).
- [57] A. Kormányos, V. Zólyomi, V. I. Fal'ko, and G. Burkard, *Phys. Rev. B* **98**, 035408 (2018).
- [58] J. Kim, K. W. Kim, D. B. Shin, S. H. Lee, J. Sinova, N. Park, and H. Jin, *Nat. Commun.* **10**, 3965 (2019).
- [59] B. Huang, G. Clark, D. R. Klein, D. MacNeill, E. Navarro-Moratalla, K. L. Seyler, N. Wilson, M. A. McGuire, D. H. Cobden, D. Xiao, W. Yao, P. Jarillo-Herrero, and X. Xu, *Nat. Nanotechnol.* **13**, 544 (2018).
- [60] C.-G. Duan, J. P. Velev, R. F. Sabirianov, Z. Zhu, J. Chu, S. S. Jaswal, and E. Y. Tsymlal, *Phys. Rev. Lett.* **101**, 137201 (2008).
- [61] E. Bousquet, N. A. Spaldin, and K. T. Delaney, *Phys. Rev. Lett.* **106**, 107202 (2011).
- [62] A. Malashevich, S. Coh, I. Souza, and D. Vanderbilt, *Phys. Rev. B* **86**, 094430 (2012).